Paper E

An Operator Algebraic Inverse Scale Space Method for Matrix Images*

* Preprint, submitted to proceedings of the 2nd Dagstuhl workshop on Visualization and Processing of Tensor Fields.

An Operator Algebraic Inverse Scale Space Method for Matrix Images

Johan Lie, Bernhard Burgeth, and Oddvar Christiansen

[1] University of Bergen Johan.Lie@cipr.uib.no
[2] University of Saarland Burgeth@mia.uni-saarland.de
[3] University of Bergen Oddvar.Christiansen@math.uib.no

Summary. During the last few years a considerable amount of research has been conducted to study multiscale properties of images via partial differential equations. In this context we can roughly divide the methodology into three different formulations, namely the scale space formulation, the regularization formulation and the inverse scale space formulation. In this work we propose an inverse scale space formulation for matrix valued images using the operator-algebraic approach recently introduced in [6, 7]. We perform numerical experiments on synthetic tensor fields and on real diffusion tensor data from DT-MRI of a human brain.

1 Introduction

In many applications there is a need for a multiscale representation of images. Partial differential equations (PDEs) provide a flexible framework for this purpose [19, 27, 8]. Traditionally, PDEs have been used via two intrinsically related approaches, namely by parabolic equations of diffusive nature and elliptic equations corresponding to the minimum of energy functionals. In between these two approaches we find the inverse scale space approach, which we will address in this paper. Inverse scale space methods have earlier been studied to some details in the context of scalar valued images [22, 5, 18, 14]. In this paper we extend the so-called *relaxed inverse scale space flow* to matrix valued images via the operator algebraic framework recently introduced in the papers [6, 7].

In this paper we consider a matrix field as a mapping $F : \Omega \subset \mathbb{R}^d \longrightarrow M_n(\mathbb{R})$, from a d-dimensional image domain into the set of $n \times n$-matrices with real entries, $F(x) = (f_{p,q}(x))_{p,q=1,\ldots,n}$. Essential for us is the subset of symmetric matrices $\mathrm{Sym}_n(\mathbb{R})$. The set of positive (semi-) definite matrices, denoted by $\mathrm{Sym}_n^{++}(\mathbb{R})$ (resp., $\mathrm{Sym}_n^{+}(\mathbb{R})$), consists of all symmetric matrices A with $\langle v, Av\rangle := v^\top Av > 0 \quad (\text{resp.}, \geq 0) \quad \text{for} \quad v \in \mathbb{R}^n \setminus \{0\}$.

Matrix fields play a vital role in many applications: In image processing itself in form of the concept of the structure-tensor [12], in civil engineering where tensors are widely used to describe anisotropic behaviour, such as strain-stress or permittivity tensors. But most importantly in this setting: medical imaging. Diffusion tensor magnetic resonance imaging (DT-MRI) [1] constitutes a modern and widely used

image acquisition technique that measures a 3×3 matrix field with positive definite matrices. To each voxel a so-called diffusion tensor is assigned describing diffusive properties of water molecules; thus it is intimately related to the geometry and organization of the tissue under examination. Hence the matrix field obtained is a valuable source of in vivo information about the underlying tissue structure e.g. in the human brain [20, 2]. This information can for example be used for the construction of maps of the tissue-connectivity [29, 30, 17], or for construction of anisotropy measures like the fractional anisotropy (FA), the relative anisotropy (RA) and the barycentric index [28]. The fractional anisotropy is a measure which is routinely used by the medical practitioners.

The indicated variety of applications requires the development of appropriate tools for the processing and analysis of matrix-valued data. Comprehensive survey articles on the analysis of DT-MRI matrix fields using various techniques can be found in [27]. The work here concentrates on the the multistage representation of matrix fields via the inverse scale space methodology.

In the context of scalar images we can write a standard parabolic flow as

$$\begin{aligned} u_t &= -p(u), \\ u(x,0) &= f, \end{aligned} \tag{1}$$

and the corresponding elliptic flow as

$$\begin{aligned} u_t &= -p(u) + \lambda(f-u), \\ u(x,0) &= f, \end{aligned} \tag{2}$$

with appropriate boundary conditions and f is the initial data. The symbol $p(u)$ denotes an differential operator involving u, usually stemming from a regularization functional. In the literature

$$p(u) = -\Delta u$$

and

$$p(u) = -\mathrm{div}\left(\frac{\nabla u}{|\nabla u|}\right)$$

are used as canonical linear and nonlinear operators respectively. In applications, often the nonlinear operators are preferable, since linear operators tend to oversmooth the edges in the images [21, 19, 8].

As indicated by the names of the two flows, the parabolic PDE (1) develops the initial condition towards the mean value of u as time increases, while the elliptic PDE (2) governs a evolution from the initial condition towards a nontrivial steady-state. In order to make the two flows meaningful, a parameter estimation must be done. In the context of the parabolic flow a stopping condition must be imposed, and in the context of the elliptic flow the weighting factor λ must be chosen. Finding the optimal parameter λ^* or t^* is in general difficult, however, approximations are usually easier to obtain.

By a proper modification of the flow (2) we get the relaxed inverse scale space flow

$$\begin{aligned} u_t &= -p(u) + \lambda(f-u+v), \\ v_t &= \alpha(f-u), \\ u(x,0) &= \mathrm{mean}(f), \\ v(x,0) &= 0, \end{aligned} \tag{3}$$

with $\alpha \leq \frac{\lambda}{5}$ as a relaxation parameter. This relaxed inverse scale space flow was first introduced by Gilboa et. al, and has been studied by several authors [5, 14]. Contrary to the standard scale space formulation, here interpreted as the flow 1, the relaxed inverse flow produces a family of images evolving from a very smooth initial condition mean(f) towards the data f. For a more detailed explanation of the inverse scale space methods, see eg. [5, 14].

Attempts to extend the PDE methodology used for scalar images to the the setting of matrix fields with positive (semi-)definite matrices have been made in [11, 24, 26, 23, 4, 25, 10]. Matrix field regularisation as suggested in [9] is based on differential geometric considerations. Recently, Christiansen et.al generalized the vector TV model of Blomgren and Chan in a straight forward manner to yield a regularization method for matrix valued images [3, 10]. This approach is interesting in the sense that during the flow, the diffusion tensor is by construction positive definite, which is usually required in DT-MRI applications.

A different and more general approach was presented in [6, 7]. There they introduced an operator algebraic approach for the construction of matrix-valued PDEs for matrix fields. They show that it is possible to transfer the characteristic behaviour of scalar operators to matrix operators as well. Important scalar models like motion by mean curvature, self-snakes, the Perona-Malik model and the ROF model are generalized to matrix valued models. And by different choices of matrix products, they preserve intrinsic matrix properties like for example positive definiteness. In [6, 7] various instances of the parabolic equation (1) are studied within this context. The setup provides a coupling of the different matrix channels treating diagonal and off-diagonal elements in a proper manner. This appropriate channel interaction is a key issue in the processing of matrix fields. As a proof-of-concept we demonstrate in this paper that the same operator-algebraic framework can be sucessfully used to obtain a relaxed inverse scale space flow (3) for matrix fields.

This chapter is organised as follows. The next section is devoted to the basic operations of the operator algebraic framework and we show how it can be used for the purpose of generalizing the inverse scale space methods to a matrix-valued setting. We discuss numerical implementation issues in section 4 Section 4 also contains a validation of our matrix-valued inverse scale space methodology by performing numerical computations on synthetic diffusion tensor fields and real DT-MRI fields. Summarizing remarks in section 5 concludes the chapter.

2 Inverse Methods for Matrix Valued Images

In this section we give a sufficiently detailed description of how we generalize the relaxed inverse scale space method from a scalar setting to a matrix setting. Although the operator-algebraic framework has been described in [6, 7] we repeat its necessary parts here for the sake of completeness.

The definition of a function of a symmetric matrix is well established in linear algebra [13]:

$$g(U) := V^\top \mathrm{diag}(g(\lambda_1), \ldots, g(\lambda_n))V$$

where $U := V^\top \mathrm{diag}(\lambda_1, \ldots, \lambda_n)V$ is the spectral decomposition of U and g is a real function applicable to the set of real eigenvalues of U. The usual product of two symmetric matrices is in general no longer symmetric unless they commute.

Hence a suitable 'symmetric' multiplication has to be found. Among the numerous possibilities we mention two choices. The so-called Jordan product is given by

$$A \bullet_J B := \frac{1}{2}(AB + BA).$$

The preconditioner product, named after its usage in numerical linear algebra as a way to precondition symmetric linear systems, is defined as

$$A \bullet_P B := \sqrt{A}B\sqrt{A}\,.$$

with a positive semidefinite A.

In the numerical experiments in this chapter we use the Jordan product, from now on simply denoted by "$\bullet$".

The rather obvious matrix-valued version of a difference quotient for a matrix fields U gives rise to a component-wise definition of **spatial or temporal partial derivatives** [6, 7]

$$\overline{\partial}_\omega U(\omega_0) = \lim_{h\to 0} \frac{U(\omega_0 + h) - U(\omega_0)}{h} = \left(\partial_\omega u_{ij}(\omega_0)\right)_{ij}. \tag{4}$$

It is close at hand that other linear operators like the arithmetic mean or convolution with a kernel are also interpreted component-wise in the matrix setting.

The set of spatial partial derivatives forms the spatial **gradient** for matrix fields $\overline{\nabla} U \in (\mathrm{Sym}_n(\mathbb{R}))^d$

$$\overline{\nabla} U(x) = \left[\overline{\partial}_{x_1} U(x), \overline{\partial}_{x_2} U(x), \cdots, \overline{\partial}_{x_d} U(x)\right]^T. \tag{5}$$

Note that this gradient is an element of the module $(\mathrm{Sym}_n(\mathbb{R}))^d$ rather than a higher order tensor as one might expect from a differential geometric point of view. We refer to a function with values in $(\mathrm{Sym}_n(\mathbb{R}))^d$ as a module field. Similarly, the generalized **divergence** defined by

$$\overline{\mathrm{div}}\ (A(x))^\top := \sum_{i=1}^{d} \overline{\partial}_{x_i} A_i(x)$$

for a module field $A(x) := \big(A_1(x), \ldots, A_d(x)\big)$ is again not a higher order tensor but simply a symmetric matrix. The definition of a **Laplacian** for a matrix field U is straight forward:

$$\overline{\Delta} U := \sum_{i=1}^{d} \overline{\partial}_{x_i}^2 U$$

Finally, there is a notion of p-**length** in the module $(\mathrm{Sym}_n(\mathbb{R}))^d$ realized for a 'fat vector' $W = (W_1, \ldots, W_d) \in (\mathrm{Sym}_n(\mathbb{R}))^d$ by

$$|W|_p := \sqrt[p]{|W_1|^p + \cdots + |W_d|^p} \in \mathrm{Sym}_n^+(\mathbb{R}).$$

The most essential term in equations (1), (2) and (3) is $p(u)$. In its most basic (linear) form we have

$$p(u) = -\sum_{i=1}^{d} \partial_{x_i}\partial_{x_i} u = -\Delta u\,. \tag{6}$$

Using the operator algebraic framework $p(u)$ can be readily generalized to an operator acting on a matrix by

$$P_\Delta(U) = -\overline{\Delta} U. \tag{7}$$

However, the linear model is not very interesting for most practical purposes. The canonical nonlinear model where the Laplacian is replaced with the nonlinear term

$$p(u) = -\mathrm{div}\left(\frac{\nabla u}{|\nabla u|}\right) \tag{8}$$

can similarly be generalized to a matrix valued setting by

$$P_{TV}(U) = -\overline{\mathrm{div}}\left(\frac{1}{|\overline{\nabla} U|} \bullet \overline{\nabla} U\right), \tag{9}$$

where $|\overline{\nabla} U|$ stands for the 2-length of $\overline{\nabla} U$, that is, $|\overline{\nabla} U| := |\overline{\nabla} U|_2 = \sqrt{\sum_{i=1}^{d} |U_i|^2}$ and "$\bullet$" denotes either the Jordan or the preconditioning product. The diffusivity can be interpreted as the inverse of $|\overline{\nabla} U|$:

$$G = \frac{1}{|\overline{\nabla} U|} = |\overline{\nabla} U|^{-1} \tag{10}$$

since we have

$$|\overline{\nabla} U|^{-1} \bullet_J |\overline{\nabla} U| = |\overline{\nabla} U|^{-1} \bullet_P |\overline{\nabla} U| = |\overline{\nabla} U|^{-1} \cdot |\overline{\nabla} U| = I\,. \tag{11}$$

Having defined the regularization operator $P(U)$ (where P equals e.g P_Δ or P_{TV}) for a matrix valued image U, we rewrite the relaxed inverse scale space flow to matrix valued images by

$$\begin{aligned} U_t &= -P(U) + \lambda(F - U + V), \\ V_t &= \alpha(F - U), \\ U(x,0) &= \mathrm{simp}(F) \\ V(x,0) &= 0, \end{aligned} \tag{12}$$

with $\alpha \leq \lambda/5$ and U, F and V being matrix fields mapping $\mathbf{R}$ to $\mathrm{Sym}_n(\mathbb{R})$. Temporal derivatives are denoted for brevity as U_t and V_t. The expression $\mathrm{simp}(F)$ stands for a simplified version of F. In the simplest case $\mathrm{simp}(F)$ might be the arithmetic mean of the matrix field F,

$$\mathrm{simp}(F) = \int_\Omega F(x)\; d\,x$$

or alternatively the solution $(x,t) \mapsto W(x,t)$ of another evolution process such as linear, Perona-Malik- or TV- diffusion. The initialization flow can for example start with initial value F and stop at a certain time τ:

$$\mathrm{simp}(F) = W(\cdot, \tau)\,.$$

From the scalar system (3) we know that with increasing time u flows from $\mathrm{simp}(f)$ towards f. Analogously, in the matrix valued setting, the flow (12) evolves from the simplified field $\mathrm{simp}(F)$ towards the matrix field F.

3 Numerical Implementation

In this section we include details on the numerical implementation of the method. We discretize the equation system (12) by standard finite differences. We employ the same numerical scheme as in [6]. Super- and sub-indexes denotes temporal and spatial discretization respectively. For the temporal derivative we use an Euler explicit scheme, i.e.

$$\frac{\partial U}{\partial t} \approx \frac{U^{n+1}_{i,j,k} - U^{n}_{i,j,k}}{\Delta t}. \tag{13}$$

To simplify the notation we sometimes omit one of the indexes. Thus we denote $U^n_{i,j,k}$ as $U_{i,j,k}$, or $U^n_{i,j,k}$ as U^n. The arithmetic mean of the diffusivity in the direction determined by the index is defined as

$$G_{i\pm\frac{1}{2},j,k} = \frac{G_{i\pm1,j,k} + G_{i,j,k}}{2}. \tag{14}$$

As a numerical approximation to P we employ $\tilde{P}$ given by

$$\begin{aligned}
\tilde{P}(U) = &\frac{1}{\Delta x}\Big(G_{i+\frac{1}{2},j,k} \bullet \frac{U_{i+1,j,k} - U_{i,j,k}}{\Delta x} - G_{i-\frac{1}{2},j,k} \bullet \frac{U_{i,j,k} - U_{i-1,j,k}}{\Delta x}\Big),\\
+ &\frac{1}{\Delta y}\Big(G_{i,j+\frac{1}{2},k} \bullet \frac{U_{i,j+1,k} - U_{i,j,k}}{\Delta y} - G_{i,j-\frac{1}{2},k} \bullet \frac{U_{i,j,k} - U_{i,j-1,k}}{\Delta y}\Big),\\
+ &\frac{1}{\Delta z}\Big(G_{i,j,k+\frac{1}{2}} \bullet \frac{U_{i,j,k+1} - U_{i,j,k}}{\Delta z} - G_{i,j,k-\frac{1}{2}} \bullet \frac{U_{i,j,k} - U_{i,j,k-1}}{\Delta z}\Big).
\end{aligned}$$

This leads to the following numerical schemes for the equation system (12)

$$\begin{aligned}
U^{n+1} &= U^n - \Delta t\Big(\tilde{P}(U^n) + \lambda(F - U^n + V^n)\Big),\\
V^{n+1} &= V^n - \alpha\Delta t(F - U^n),\\
U^0 &= \mathrm{simp}(F),\\
V^0 &= 0.
\end{aligned} \tag{15}$$

We will use the numerical schemes introduced above to perform numerical experiments on matrix fields in the next section.

4 Numerical Experiments

Numerical experiments on artificial and real DT-MRI data will confirm that the inverse scale space concept can be transfered to the matrix fields via the operator-algebraic framework. For all the numerical experiments we initialize the algorithm with an over-smoothed version of the noisy matrix field F, $U(x,0) = \mathrm{simp}(F)$, as described in section 2. From the simplified matrix field $U(x,0)$ the matrix field $U(x,t)$ evolves towards the noisy matrix field F. All the processed matrix fields are 3D matrix fields, however, we display only one 2D-slice of the data set.

All computations are done on a computer with a 2 Opteron 270 Dual-core processor and 8 GB of memory. The implementation is done in matlab with some parts implemented in C using mex files [15].

A simple synthetic field

In the first numerical experiment we apply the proposed methodology on a simple three-dimensional tensor field with spatial dimensions $16 \times 16 \times 5$. All five layers in this data set are equal, and Figure 1(a) shows one slice of the tensor field. The tensor field consists of two regions, one with principal diffusion direction along the east-west and one along the north-south direction. Each matrix in the regions have one single large eigenvalue of 1, and two small eigenvalues of 0.25. Thus the regions are highly anisotropic.

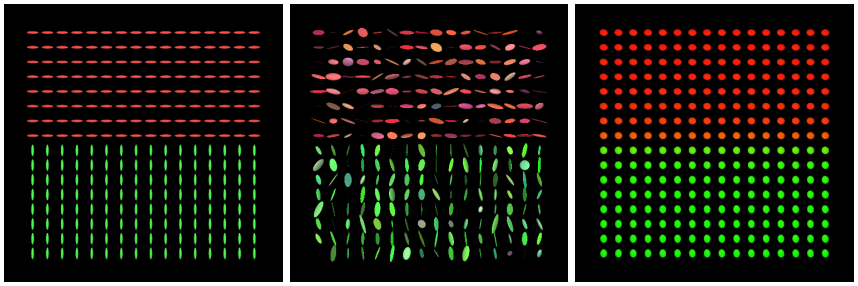

(a) (b) (c)

Fig. 1. (a) A simple synthetic field with two regions. (b) Normal distributed noise with zero mean and variance of 0.2 is added to the clean tensor field. (c). The noisy tensor field is evolved, using a simple forward model, into an over-smoothed tensor field.

The clean tensor field has matrix elements in the range from 0 to 1, and we add normal distributed noise with zero mean and variance of 0.2, see Figure 1(b). This tensor field is then evolved, using a simple forward model, into an over-smoothed tensor field, see Figure 1(c). The noisy tensor field and the over-smoothed tensor field is then respectively used as the input parameters F and $\mathrm{simp}(F)$ in (12).

In Figure. 2 we observe that more and more information is added to U as time progresses. After a while the field is almost identical to the noise-free field. And as antisipated, a while after this, the noise reappears in the field U. Eventually, $U \to F$ as $t \to \infty$, which also is to be expected.

A more complex synthetic example

In the next example we have a more complex synthetic three-dimensional tensor field with spatial dimensions $32 \times 32 \times 5$. As in the previous example all five layers are equal, and Figure 3(a) shows one slice of the tensor field. The tensor field consists of four regions, the outermost region is empty with each matrix equal to the null matrix. The second outermost region is circle shaped. Each matrix in this region has two large eigenvalues of 1 and a single small one of 0.25. The two innermost regions are more anisotropic. Each matrix in these regions have one single large eigenvalue of 1 and two smaller ones of 0.25.

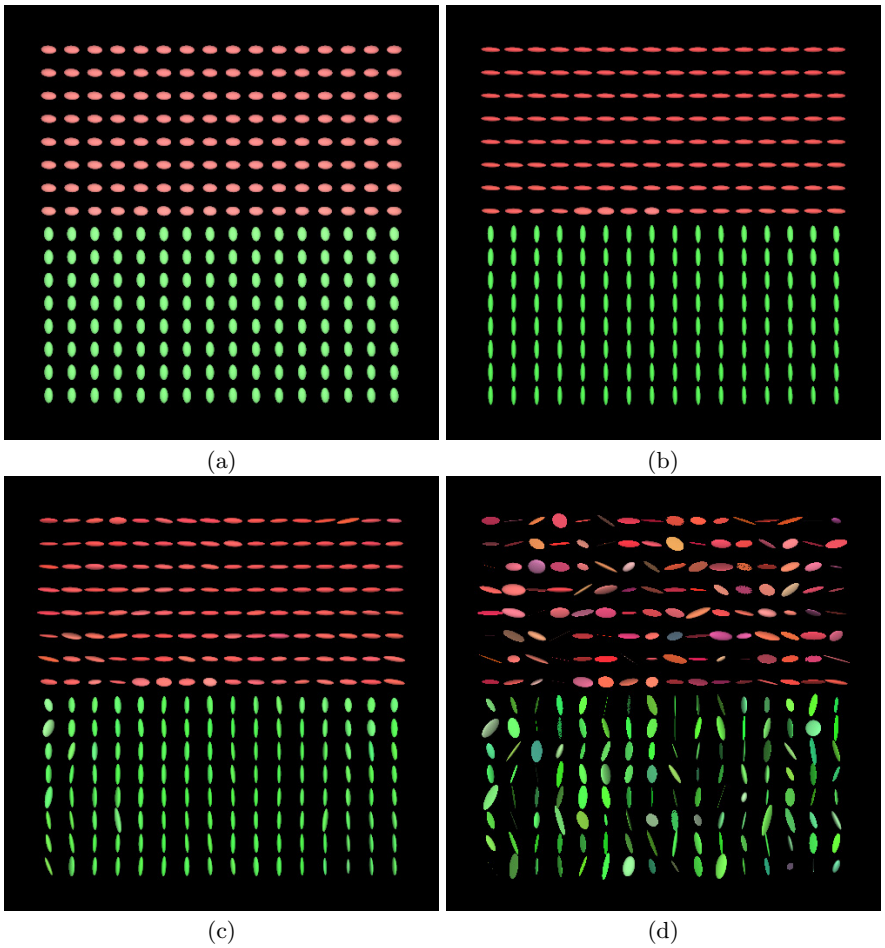

Fig. 2. The relaxed inverse scale space flow in a matrix setting. (a) After 300 iterations the over-smoothed tensor field has started to align along the directions in the true solution. (b) After 1950 iterations we are close to the true solution. (c) After 5000 iterations noise is beginning to appear in the matrix field. (d) After 20000 iterations U is close to the noisy data F.

The clean tensor field has matrix elements in the range from 0 to 1, and we add normal distributed noise with zero mean and variance of 0.2, see Figure 3(b). This tensor field is then evolved, using a simple forward model (ROF model with $\lambda = 0$), into an over-smoothed tensor field, see Figure 3(c). The noisy tensor field and the over-smoothed tensor field are then used as the input parameters F and simp(F) respectively in (12).

As in the previous example we observe that more and more information is added to U as time increases, see Fig. (4). As anticipated the evolution from a degraded

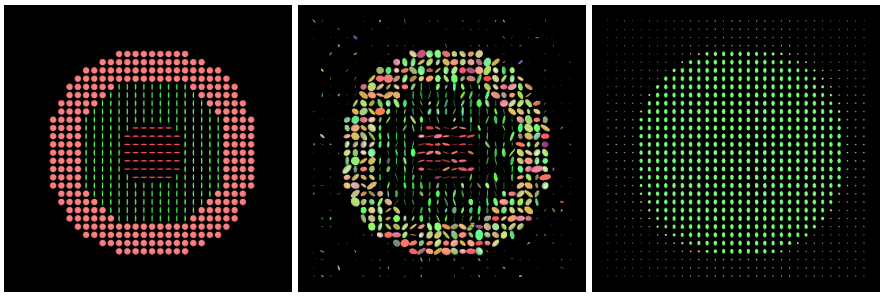

(a) (b) (c)

Fig. 3. (a) A more complex synthetic field with four regions. (b) Normal distributed noise with zero mean and variance of 0.2 is added to the clean tensor field. (c). The noisy tensor field is evolved, using a simple forward model, into an over-smoothed tensor field.

image over a somewhat denoised version to a variant close to the polluted version is observed.

By these experiment we have demonstrated that at least qualitatively the relaxed inverse scale space flow in the matrix setting indeed behaves as expected from the scalar setting. The diffusion tensors field evolves from an essentially isotropic tensor field at $t = 0$, through a state of a structured anisotropic tensor field, and finally towards a noisy unstructured anisotropic tensor field.

Real Brain DTI

In the last numerical experiment we apply the proposed methodology on a real diffusion tensor MRI tensor field. To be able to display a slice of the complex human brain tensor field as a whole, we use a color-coded FA plot instead of the ellipsoid representation used in the previous experiments, see Figure 5(a). However, the calculations are performed, as before, on the underlying matrix field.

The data used is a full 3D matrix valued data set with spatial dimensions $110 \times 126 \times 65$. The human subject data were acquired using a 3.0 T scanner (Magnetom Trio, Siemens Medical Solutions, Erlangen, Germany) with a 8-element head coil array and a gradient subsystem with the maximum gradient strength of 40 $\mathrm{mT{\cdot}m^{-1}}$ and maximum slew rate of 200 $\mathrm{mT{\cdot}m^{-1}{\cdot}ms^{-1}}$. The DTI data were based on spin-echo single shot EPI acquired utilizing generalized auto calibrating partially parallel acquisitions (GRAPPA) technique with acceleration factor of 2, and 64 reference lines. The DTI acquisition consisted of one baseline EPI, S_0, and six diffusion weighted images $S_1, \ldots, S_6$ (b-factor of 1000 $\mathrm{s{\cdot}mm^{-2}}$) along the same gradient directions as in the previous example. Each acquisition had the following parameters: TE / TR / averages was 91 ms / 10000 ms / 2, FOV was 256 mm×256 mm, slice thickness / gap was 2 mm / 0 mm, acquisition matrix was 192×192 pixels and partial Fourier encoding was 75%.

Since we are working with real data we do not have access to an exact "true" solution. Instead we used a high quality reference dataset for comparison, see Figure 5(b). This dataset was obtained by registering and averaging 18 acquisitions.

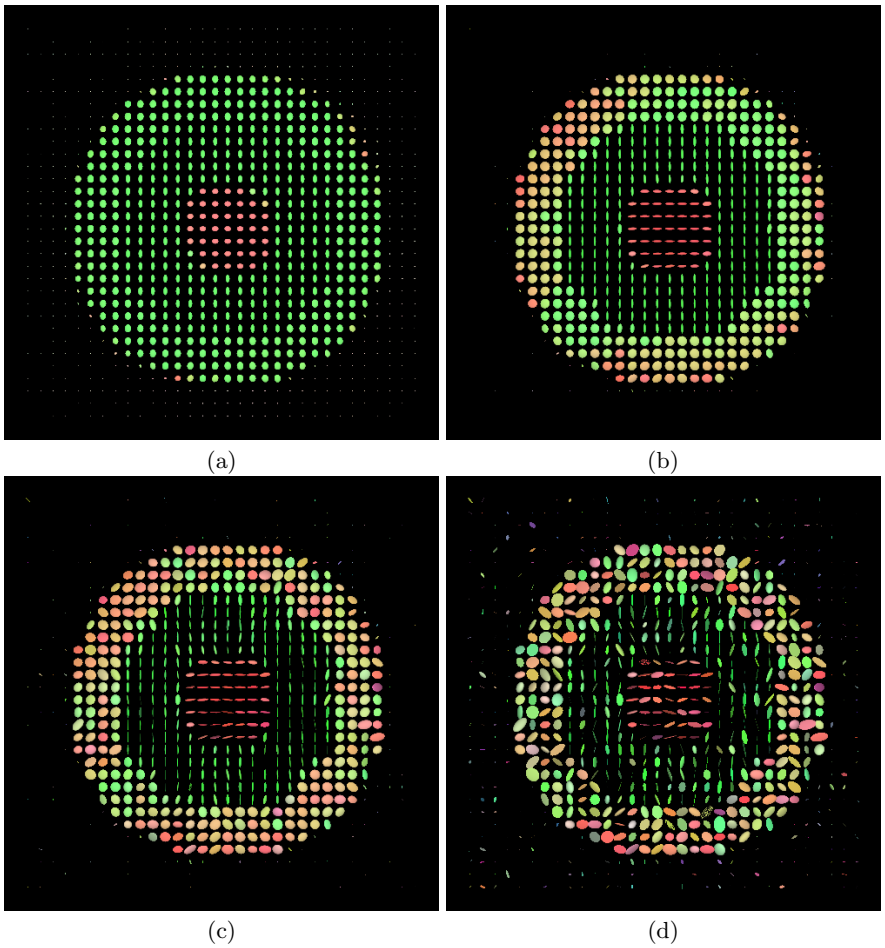

Fig. 4. The relaxed inverse scale space flow in a matrix setting. (a) After 500 iterations the over-smoothed tensor field has started to align along the directions in the true solution. (b) After 2430 iterations we are close to the true solution. (c) After 5000 iterations noise is beginning to appear in the matrix field. (d) After 20000 iterations U is close to the noisy data F.

The noisy dataset used as F in (12) is a 4 averaged acquisitions consuming about 20% of the acquisition time, compared to the higher-quality one. This dataset is then evolved into an over-smoothed dataset and used as the initial parameter simp(F), see Figure 5(c).

From the experiment, see Figure 6 we clearly see that the inverse scale space methodology is well suited for the construction of multiscale representations of DTMRI fields of the human brain. The visualizations are made by the software DTIStudio, which is developed by Mori et.al [16].

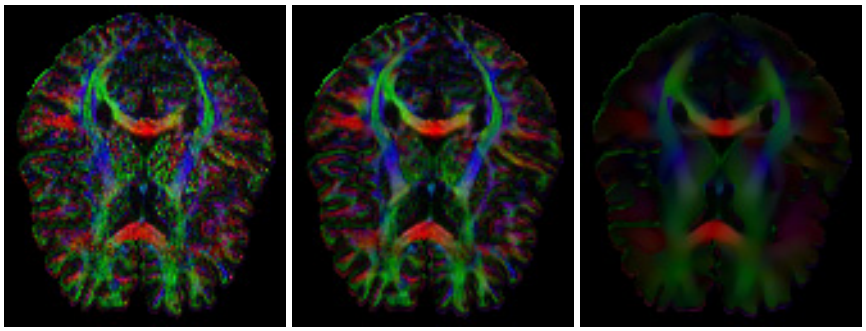

(a) (b) (c)

Fig. 5. Color coded FA plots of one slice of real DTI (a) The noisy input image. (b) High quality reference solution where 18 measurements are registered and averaged. (c). The noisy tensor field evolved into an over-smoothed tensor field.

5 Conclusions

In this paper we have employed the operator-algebraic framework of Burgeth et.al to make a straight forward generalization of the so-called relaxed inverse scale space flow to matrix images. We have performed numerical experiments which indicates that the matrix flow qualitatively resembles the scalar flow.

6 Acknowledgements

We want to thank Stephan Didas for providing the data for this project, and for kindly helping us with the visualization of the tensor fields. The visualization of the tensor fields was done by an in-house visualization software from the Mathematical Imaging and Analysis group at Saarland University. We also would like to thank Dr. Siamak Ardekani at UCLA for kindly providing the real DTMRI data used in this project.

References

1. P. J. Basser, J. Mattiello, and D. LeBihan. MR diffusion tensor spectroscopy and imaging. *Biophysical Journal*, 66:259–267, 1994.
2. P.J Basser, J. Mattiello, and D. LeBihan. MR diffusion tensor spectroscopy and imaging. *Biophysical Journal*, 66(1):259–267, 1994.
3. P. Blomgren and T.F Chan. Color TV: Total variation methods for restoration of vector-valued images. *IEEE Transactions on Image Processing*, 7(3):304–309, 1998.
4. T. Brox, J. Weickert, B. Burgeth, and P. Mrázek. Nonlinear structure tensors. *Image and Vision Computing*, 24(1):41–55, 2006.

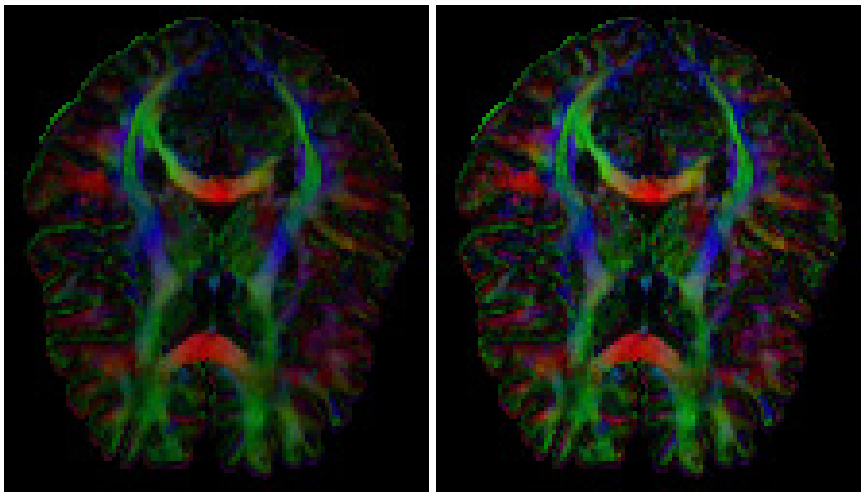

(a)

(b)

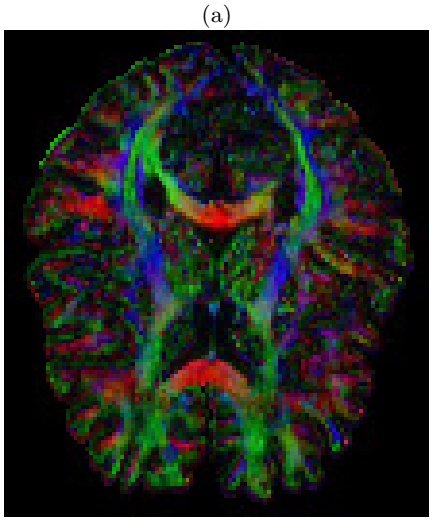

(c)

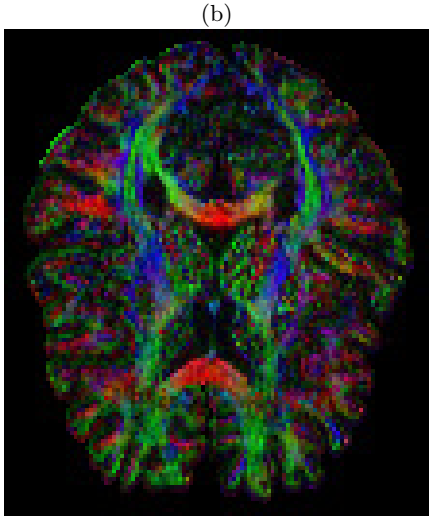

(d)

Fig. 6. One slice of a real diffusion tensor field of a human brain, color-coded FA plot. (a) After 50 iterations we are approaching a good result. (b) After 110 iterations we are close to the optimal matrix field. (c) After 250 iterations noise is beginning to appear in the matrix field. (d) After 1000 iterations U is close to the noisy data F.

5. Martin Burger, Guy Gilboa, Stanley Osher, and Jinjun Xu. Nonlinear inverse scale space methods. *Communications in Mathematical Sciences*, 4(1):179–212, 2006.
6. Bernhard Burgeth, Stephan Didas, Luc Florack, and Joachim Weickert. A Generic Approach to Diffusion Filtering of Matrix-Fields. *Universität des Saarlandes, Fachrichtiung 6.1 Mathematik, Preprint*, 191, 2007.
7. Bernhard Burgeth, Stephan Didas, Luc Florack, and Joachim Weickert. A Generic Approach to the Filtering of Matrix Fields with Singular PDEs. *Preprint*, 2007.
8. Tony F. Chan and Jianhong Shen. *Image Processing And Analysis: Variational, PDE, Wavelet, And Stochastic Methods*. SIAM, 2005.
9. C. Chefd'Hotel, D. Tschumperlé, R. Deriche, and O. Faugeras. Constrained flows of matrix-valued functions: Application to diffusion tensor regularization. In A. Heyden, G. Sparr, M. Nielsen, and P. Johansen, editors, *Computer Vision – ECCV 2002*, volume 2350 of *Lecture Notes in Computer Science*, pages 251–265. Springer, Berlin, 2002.
10. Oddvar Christiansen, Tin-Man Lee, Johan Lie, Usha Sinha, and Tony F. Chan. Total variation regularization of matrix valued images. *To appear in International Journal of Biomedical Imaging, special issue on Mathematics in Biomedical Imaging*, (June 2007).
11. C. Feddern, J. Weickert, B. Burgeth, and M. Welk. Curvature-driven PDE methods for matrix-valued images. *International Journal of Computer Vision*, 69(1):91–103, August 2006.
12. W. Förstner and E. Gülch. A fast operator for detection and precise location of distinct points, corners and centres of circular features. In *Proc. ISPRS Intercommission Conference on Fast Processing of Photogrammetric Data*, pages 281–305, Interlaken, Switzerland, June 1987.
13. R. A. Horn and C. R. Johnson. *Matrix Analysis*. Cambridge University Press, Cambridge, UK, 1990.
14. Johan Lie and Jan M. Nordbotten. Inverse scale spaces for nonlinear regularization. *Journal of Mathematical Imaging and Vision*, 27(1):41–50, 2007.
15. The Mathworks., MatLab, The Language of Technical Computing. http://www.mathworks.com/matlab
16. Mori and coworkers. Dti-studio.
17. Susumi Mori and Peter C.M. van Zijl. Fiber tracking: principles and strategies - a techical review. *NMR Biomed*, 15:468–480, 2002.
18. Stanley Osher, Martin Burger, Donald Goldfarb, Jinjun Xu, and Wotao Yin. An iterative regularization method for total variation-based image restoration. *Multiscale Model. Simul.*, 4(2):460–489, 2005.
19. Stanley Osher and Ronald Fedkiw. *Level set methods and dynamic implicit surfaces*, volume 153 of *Applied Mathematical Sciences*. Springer-Verlag, New York, 2003.
20. C. Pierpaoli, P. Jezzard, P. J. Basser, A. Barnett, and G. Di Chiro. Diffusion tensor MR imaging of the human brain. *Radiology*, 201(3):637–648, December 1996.
21. L. Rudin, S. Osher, and E. Fatemi. Nonlinear total variation based noise removal algorithm. *Physica D.*, 60:259–268, 1992.
22. Otmar Scherzer and Chuck Groetsch. Inverse scale space theory for inverse problems. In M. Kerckhove, editor, *Scale-Space and Morphology in Computer*

Vision : Third International Conference, Scale-Space 2001, volume 2106 of *Lecture Notes in Computer Science*. Springer-Verlag GmbH, 2001.
23. T. Schultz, B. Burgeth, and J. Weickert. Flexible segmentation and smoothing of DT-MRI fields through a customizable structure tensor. In *Proceedings of the International Symposium on Visual Computing*, Lecture Notes in Computer Science. Springer, Berlin, 2007.
24. D. Tschumperlé and R. Deriche. Diffusion tensor regularization with constraints preservation. In *Proc. 2001 IEEE Computer Society Conference on Computer Vision and Pattern Recognition*, volume 1, pages 948–953, Kauai, HI, December 2001. IEEE Computer Society Press.
25. Z. Wang, B.C Vemuri, and Y Chenand T Mareci. A constrained variational principle for direct estimation and smoothing of the diffusion tensor field from complex dwi. *IEEE Transactions on Medical Imaging*, 23(8):930 – 939, 2004.
26. J. Weickert and T. Brox. Diffusion and regularization of vector- and matrix-valued images. In M. Z. Nashed and O. Scherzer, editors, *Inverse Problems, Image Analysis, and Medical Imaging*, volume 313 of *Contemporary Mathematics*, pages 251–268. AMS, Providence, 2002.
27. Joachim Weickert and Hans Hagen (Eds.). *Visualization and Processing of Tensor Fields*. Mathematics and Visualization. Springer, 2005.
28. C.-F Westin, S.E. Maier, H. Mamata, A. Nabavi, F.A. Jolesz, and R. Kikinis. Processing and visualization for diffusion tensor mri. *Medical Image Analysis*, 6:93–108, 2002.
29. Leonid Zhukov and Alan H. Barr. Oriented tensor reconstruction: Tracing neural pathways from diffusion tensor mri. IEEE Visualization 2002, 2002.
30. Leonid Zhukov and Alan H. Barr. Heart-muscle fiber reconstruction from diffusion tensor mri, 2003.